Journal of Power Sources 268 (2014) 414–422

Contents lists available at ScienceDirect

Journal of Power Sources

journal homepage: www.elsevier.com/locate/jpowsour

A high performance layered transition metal oxide cathode material obtained by simultaneous aluminum and iron cationic substitution

Wassima El Mofid [a], Svetlozar Ivanov [a, *], Alexander Konkin [b], Andreas Bund [a]

[a] Department of Electrochemistry and Electroplating, Technische Universität Ilmenau, D-97693 Ilmenau, Germany
[b] Center for Micro and Nanotechnologies, Technische Universität Ilmenau, D-98693 Ilmenau, Germany

HIGHLIGHTS

- Self-combustion was applied to prepare $LiNi_{0.6}Mn_{0.2}Co_{0.15}Al_{0.025}Fe_{0.025}O_2$ material.
- Rietveld refinement showed a decrease of the cationic mixing after metal substitution.
- EPR suggests a redistribution of the Ni ions in the structure after the substitution.
- $LiNi_{0.6}Mn_{0.2}Co_{0.15}Al_{0.025}Fe_{0.025}O_2$ showed an improved capacity and cycling stability.

ARTICLE INFO

Article history:
Received 22 March 2014
Received in revised form
23 May 2014
Accepted 9 June 2014
Available online 15 June 2014

Keywords:
Li-ion battery
Cathode
NMC
Electron paramagnetic resonance
Cation exchange

ABSTRACT

The method of self-combustion synthesis was applied to prepare double Al- and Fe-substituted $LiNi_{0.6}Mn_{0.2}Co_{0.15}Al_{0.025}Fe_{0.025}O_2$ (NMCAF) and non-substituted $LiNi_{0.6}Mn_{0.2}Co_{0.2}O_2$ (NMC-3:1:1) cathode materials for lithium ion batteries. The novel NMCAF structure obtained by simultaneous cationic substitution showed an improved capacity and high stability during electrochemical cycling. X-ray diffraction patterns proved that both materials have a layered α-$NaFeO_2$ type structure with a good hexagonal ordering. It was found that NMCAF has increased *a* and *c* lattice parameters due to a structural expansion caused by Al and Fe ion substitution. Rietveld refinement analysis revealed a significant decrease of the cationic mixing after the metal substitution, suggesting a structural stabilization. Electron paramagnetic resonance (EPR) spectroscopy showed that Al and Fe substitution markedly influenced the EPR spectrum of NMC-(3:1:1). The EPR spectral lines of both materials are attributed to Mn^{4+} and Ni^{2+} present in the structure. The change in the Ni^{2+} line after the metal substitution suggests a redistribution of the Ni ions in the structure, which can be related to the diminished cation mixing in the NMCAF. The improved electrochemical behavior of NMCAF is closely connected to the stabilization of the layered structure and the reduction of the cation mixing after metal substitution.

1. Introduction

Due to their high energy and power density, lithium-ion batteries (LIB)s are widely used in small portable electronic devices and more recently in electric vehicles. $LiCoO_2$ was for a long time a leading cathode material integrated worldwide in different types of consumer electronics. However, the increasing requirements for high power and energy LIBs, the relatively high cost of $LiCoO_2$, environmental and safety issues limit its further large scale application [1]. In the recent years, $LiNi_xMn_yCo_{1-x-y}O_2$ (NMC), a transition-metal oxide with analogous layered structure to that of $LiCoO_2$, has gained considerable recognition as a potential substitute for $LiCoO_2$ [1–3]. Particular positive features of this material are lower cost, less toxicity, improved rate capability and thermal stability. Due to its higher practical reversible capacity NMC displays good cycling performance [1,2].

In contrast to $LiCoO_2$, NMC has a flexible stoichiometry by which the electrochemical performance of the material can be adjusted. The most widely researched NMC composition $LiNi_{0.33}Mn_{0.33}Co_{0.33}O_2$ (NMC-1:1:1), having a hexagonal structure, was initially introduced by Ohzuku's group in 2001 and was further established as the most promising in this class of materials [3]. It was found that whereas the NMC capacity grows with the increase of Ni content, to maintain the structural and thermal stability of Ni reach NMC materials is challenging [4]. Nevertheless, the structure and composition of NMC with higher Ni content can be further optimized to adjust the stability and the electrochemical performance

* Corresponding author.
E-mail address: svetlozar-dimitrov.ivanov@tu-ilmenau.de (S. Ivanov).

http://dx.doi.org/10.1016/j.jpowsour.2014.06.048
0378-7753/

of the material. An example is NMC-(3:1:1) which has not been extensively studied. Furthermore, similar to other compositions [5], there is a high expectation that the properties of NMC-(3:1:1) can be adjusted in order to improve the stability and performance of the structure. In particular, further Fe and Al substitution can offer increased stability, reduction of the environmental risk by bringing into play a smaller amount of cobalt, reduction of the cost and ensure high specific capacity by the increased amount of nickel.

It was established that the process of Li ion exchange in the structure of NMC takes place by reaction involving Ni^{2+}/Ni^{4+} and Co^{3+}/Co^{4+} redox couples, whereas Mn^{4+} ions do not undergo chemical transformation and play a central role for the structural stability. An important condition for the safe operation of NMC materials is the preservation of their exact layered structure, where efficient solid state diffusion of Li^+ is ensured in firmly alternating planar geometry. Nevertheless, it has been shown that the cation mixing between Li and Ni ions on the crystallographic 3b site of the NMC lattice has a negative effect on the structural stability and further affects the electrochemical performance of layered oxides [6]. The physical reason for this phenomenon is related to the similarity between the ionic radii of Li^+ and Ni^{2+}. The ionic radius of Li^+ (0.76 Å) is close to that of Ni^{2+} (0.69 Å), hence a partial occupation of Ni^{2+} sites by Li^+ (by exchange between a Li^+ and a nearest neighbor Ni^{2+}) induces a cation mixing in the structure, which hinders the efficient Li-ion transport in the solid state [6]. Taking into account this problem, two main approaches have been implemented: cationic substitution with transition metals such as Al, Mg, Fe, Cr, etc. [7–12] and surface modification by coating with metal oxides or fluorides [13–16]. Both approaches result in less cation mixing, hence structural stability and improved electrochemical performance of the cathode material.

The cycling behavior of NMC is significantly dependent on its preparation conditions, e.g. synthetic procedure and thermal post treatment. Alternatively to hydrothermal and solid-state synthesis, the self-combustion method has advantages such as the simplicity of the procedure, the good homogeneity of the synthesized materials, and the reduction of the temperature during heat treatment, thus, the decrease of the costs. Furthermore, the self-combustion approach offers the possibility to adjust grain sizes down to the nanometer scale.

In the present study, the structural and electrochemical properties of NMC-(3:1:1) and NMCAF, obtained via simultaneous substitution of Co by Fe and Al, were analyzed in detail. The main goal of the work is to elucidate the influence of the double (Fe and Al) metal substitution on the electrochemical functional properties of the obtained material. Even though it was previously determined that metal substitution in layered materials generally brings an improved stability and performance for a number of cathode compositions, the simultaneous Al and Fe substitution has not been approached. Furthermore, it is expected that the pristine cathode material NMC-(3:1:1), which exhibits good electrochemical behavior, is promising for further Co substitution, in order to achieve a stable, environmentally benign and high performance structure. The combination of XRD and EPR spectroscopy allowed a detailed structural analysis, clarifying the physical base of the improvement of the NMC-(3:1:1) electrochemical performance after the metal substitution.

2. Experimental

2.1. Chemicals and materials

Ethylene carbonate (EC), dimethyl carbonate (DMC), $LiPF_6$, $Li(NO_3)$, $Ni(NO_3)_2$, $Co(NO_3)_2$, $Mn(NO_3)_2$, $Al(NO_3)_3$ and $Fe(NO_3)_3$ were purchased from Alfa Aesar. NMC-(1:1:1) was supplied by Sigma–Aldrich. The solvents and electrolytes necessary for electrochemical experiments were dried until a value of 15 ppm H_2O was reached. The moisture in the electrolytes was controlled by Karl–Fischer titration (831 KF Coulometer from Metrohm).

2.2. Material synthesis

NMC-(3:1:1) and NMCAF were prepared by the self-combustion synthesis method [17]. The procedure starts from aqueous solutions (1 M) of $Li(NO_3)$, $Ni(NO_3)_2$, $Co(NO_3)_2$, $Mn(NO_3)_2$, $Al(NO_3)_3$ and $Fe(NO_3)_3$. Stoichiometric amounts of these solutions are mixed with an aqueous solution of sucrose $C_{12}H_{22}O_{11}$, used as a fuel, in a crystallizer under continuous stirring. The solution is then heated by means of a sand bath to 120 °C for 2 h and gives rise to a spongy product. After a few minutes, combustion is triggered spontaneously and spreads over the surface of the foamy mass. The product is then ground mechanically by a mortar until a fine black powder is obtained. The annealing involves heating the sample to 900 °C under air, with a rate of 5 °C min^{-1}, then maintaining that temperature (900 °C) for 1 h. Afterward, the temperature is allowed to drop spontaneously down to room temperature.

2.3. Material characterization

The phase identification of NMC-(3:1:1) and NMCAF compounds was carried out by powder X-ray diffraction, using a Siemens D5000 diffractometer in reflection mode with Cu Kα radiation. XRD patterns were recorded in the 2θ range from 15 to 100° with a step size of 0.02° and a rest time of 1 s/step. The structural parameters were obtained by the Rietveld refinement method using the FullProf software [18].

The specific surface of the samples was measured by Gemini 2360 Surface Area Analyser by applying the Brunauer–Emmett–Teller (BET) theory.

Differential Thermal Analysis and Thermogravimetric analysis (DTA/TG) were performed in the temperature range from 20 to 1020 °C with a scan rate of 5 °C min^{-1}.

Particle sizes and morphology of the prepared powder were evaluated using a high-resolution scanning electron microscope (Hitachi S-4800 II).

ESR spectra were recorded by the continue wave Bruker X-band spectrometer ELEXYS E500 with 100 kHz field modulation in a temperature interval of 77–295 K. For accurate g-factors determination, a hyperfine structure (hfs) line ($m = -1/2$) of the $Cu^{2+}(dtc)_2$ complex in benzene solution (denoted as $Cu^{2+}L_2$) was used as a standard. The $Cu^{2+}L_2$ sample location in the resonator is independent on the position of the studied samples and is recorded at room temperature. Therefore, in all experiments, the above $Cu^{2+}L_2$ hfs ($m = -1/2$) has been used as reference line with g-factor position at ESR spectrum amplitude peak $g = 2.025$.

2.4. Preparation of NMC electrodes

The optimum composition for electrode preparation proved to be 75 wt.-% active material, 15 wt.-% polyvinylidene fluoride (PVDF) dissolved in *N*-methyl-2 pyrrolidone (NMP) used as binder and 10 wt.-% carbon black used as conductive agent.

The obtained slurry was deposited on Al current collectors with an automated slurry applicator ZAA 2300, Zehntner Testing Instruments. The dry thickness of the electrode coatings was controlled to be in the range of 50–60 μm. The average mass of active material was 2.70 mg cm^{-2}. The deposit was dried at 50 °C for 4 h and then cut to a size compatible for standard CR2016 coin cells. The electrodes were weighed and dried under vacuum at 120 °C for 12 h.

2.5. Electrochemical characterization

The electrolyte solution used for the electrochemical experiment consisted of 1 M $LiPF_6$ dissolved in EC (ethylene carbonate): DMC (dimethyl carbonate) (1:1 vol.-%). Metallic Li foil was used as counter electrode and Celgard polyethylene as separator. The water content of the electrolyte was monitored by means of Karl–Fischer titration and was typically 15–30 ppm. The coin cells were assembled in a glove box under a dry and high purity argon atmosphere, by means of MSK-110 Hydraulic Crimping Machine, MTI Co.

Cyclic voltammetry was carried out with a BioLogic multichannel potentiostat/galvanostat VMP3 in a PTFE home-made electrochemical cell with lithium counter and reference electrode under argon atmosphere. The voltammograms were recorded in the potential range between 2.6 and 4.5 V versus Li/Li^+ at 100 μV s^{-1}. The charge and discharge performance was characterized galvanostatically using standard CR2016 coin-type cells over a potential range between 2.5 and 4.4 V vs. Li/Li^+ for slow rates and 2.8 and 4.6 V vs. Li/Li^+ for faster rates.

3. Results and discussion

3.1. XRD analysis of material structure

The X-ray diffraction patterns of the novel positive electrode material NMCAF and the non-substituted NMC-(3:1:1), prepared by self-combustion method are shown in Fig. 1. For both materials all diffraction peaks can be indexed in the α-$NaFeO_2$ type structure (space group: $R\bar{3}m$) suggesting that the small amounts of Al and Fe substituted for Co in the starting material NMC-(3:1:1) did not affect the stability of the crystal lattice.

The narrow shape of the reflections, quantified by the full width at half maximum (FWHM) of the main reflections (003) and (104) and the splitting of the doublets (006)/(102) and (108)/(110) are considered as signs of high crystallinity and well-ordered layered structure [19,20]. The FWHM of the reflections (003) and (104) are respectively around 0.321° and 0.362° for NMCAF and around 0.427° and 0.417° for NMC-(3:1:1) (Table 1). The smaller values of the FWHM for NMCAF indicate better crystallinity than the non-substituted material and suggest a homogeneous distribution of the cations in the structure.

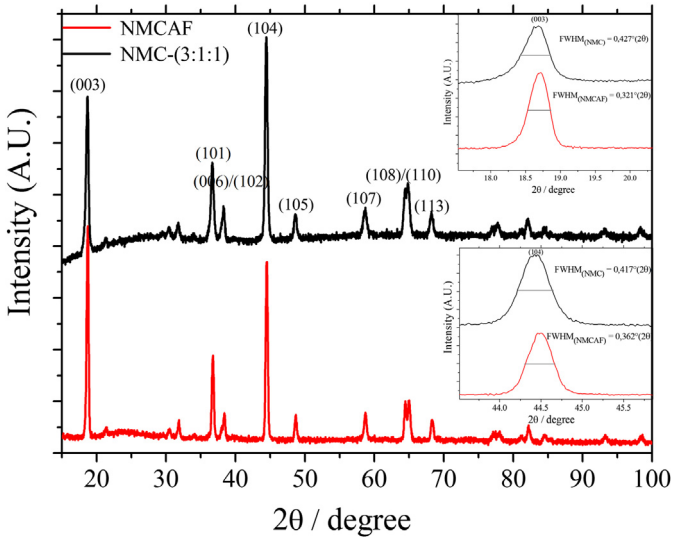

Fig. 1. X-ray diffraction patterns of NMCAF (red) and NMC-(3:1:1) (black) positive electrode materials. Insets: peak shape before and after metal substitution, (003) – up, (104) – down. (For interpretation of the references to color in this figure legend, the reader is referred to the web version of this article.)

Furthermore, the ratio of (003)/(104) reflection intensities is an important parameter for evaluation of the cation distribution in the crystal lattice [21]. It was found that the increase of this ratio is related to the decrease in the degree of the cation mixing. Accordingly, in our case, the simultaneous Fe and Al substitution of Co reduced the degree of cation mixing since the (003)/(104) ratio is higher than that of non-substituted NMC material (Table 1). The latter result suggests a possible improvement of the electrochemical performances after cationic substitution, since the decline of cation mixing degree results in a decrease of the hindrance for lithium ion diffusion in the structure. Therefore, less capacity fading during cycling is expected.

In order to evaluate in detail the deviation of the NMCAF lattice parameters after the metal substitution, the diffractograms were analyzed by means of the Rietveld refinement method. This approach consists in simulating a diffractogram from a crystallographic model of the sample – α-$NaFeO_2$ in our case and minimizing by the least squares method the difference between the simulated diffraction pattern and the measured one. The profile of the diffraction lines is described by pseudo-Voigt function, which is a linear combination of a Gaussian and a Lorentzian function. A quasi-linear minimization function between the experimental and calculated X-ray diffraction profiles was obtained (Fig. 2), which confirms the validity of the considered α-$NaFeO_2$ structural model.

Table 1 summarizes the lattice parameters calculated by Rietveld refinement of the XRD data. It can be seen that the values of the lattice parameters *a* and *c* are slightly larger for the substituted material than for the starting one. It can be further considered that the lattice expansion in the *a* and *c* directions is mainly related to the larger radius of the Fe^{3+} ion (64.5 pm) compared to that of Co^{3+} (54.5 pm). On the other hand, the influence of Al substitution on the structure could be neglected since the ionic radii of Al^{3+} (53.5 pm) and Co^{3+} (54.5 pm) are very close.

One of the refined parameters in the Rietveld method is the occupancy of Ni^{2+} on the crystallographic 3*b* site of the lattice, which is about 5% for the cationic substituted material. This amount of extra nickel is markedly inferior to that of the starting NMC material (13%), which suggests less cation mixing in the structure. Therefore better diffusion of the lithium ions and more promising electrochemical performance for NMCAF can be anticipated.

3.2. Electron paramagnetic resonance

The in-lab synthesized NMC-(3:1:1), NMCAF and commercially available NMC-(1:1:1) were analyzed by means of EPR spectroscopy in the temperature range 77 K–295 K. The experimental EPR spectra recorded at 77 K and 295 K and their corresponding best fits are presented in Fig. 3. The experimental spectra measured at the intermediate temperatures 250 K, 200 K, 150 K and 104 K (not

Table 1
Structural parameters of NMC-(3:1:1) and NMCAF obtained by XRD.

Crystal data	NMCAF	NMC-(3:1:1)	Parameters deviation in %
a (Å)	2.868	2.861	0.2
c (Å)	14.211	14.167	0.3
V (Å^3)	101.22	100.56	0.6
I(003)/*I*(104)	1.19	0.86	27.7
Occupancy of Ni^{2+} on Li^+ sites	0.05	0.13	61.5
$FWHM_{(003)}$(°)	0.321	0.427	24.8
$FWHM_{(104)}$(°)	0.362	0.417	13.2

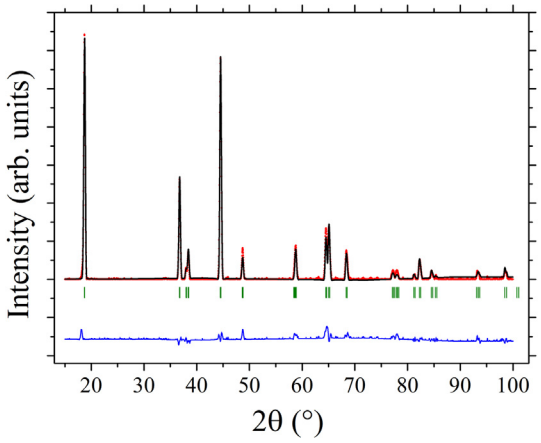

Fig. 2. Rietveld profile refinement results of NMCAF: —— observed, —— calculated, —— difference, | Bragg position.

shown here) occupy the range located between the EPR spectra at the limiting temperatures 77 K and 295 K.

The best fit of the experimental spectra was carried out by a Lorentzian line approach [22,23] and resulted in one single line for NMC-(1:1:1) and two separate EPR lines for NMC-(3:1:1) and NMCAF, represented in Fig. 4. The broad line has been attributed to paramagnetic Mn^{4+} (denoted as R_1) and the relatively narrow one (denoted as R_2) has been assigned to presence of paramagnetic Ni^{2+} defects [24]. The values of the EPR spectroscopic parameters (g_i-factors and line width ΔH_i) are displayed as a function of temperature in Fig. 4a and b, where $i = 1; 2$ relates to R_1 and R_2 correspondingly.

The width of the EPR signal ΔH_i ($i = 1; 2$) refers to a peak width at its half-height. In general, it can be observed that the decrease of the temperature is associated with an increase of ΔH_i and a decrease of the g_i-factor. As expected, for NMC-(3:1:1) and NMC-(1:1:1) the temperature dependences of g_i and ΔH_1 correlate well with data for analogous $LiNi_xMn_xCo_{1-2x}$ structures [24,25], which verifies the consistency of the EPR analysis.

It has been previously reported that the EPR line width depends strongly on the stoichiometry of the material. Recent studies established that EPR line width ΔH_1 undergoes narrowing when the Ni/Mn ratio decreases [22]. In the present experiment the results obtained for NMC-(1:1:1), ΔH_1 ~1200 G, Ni/Mn ~1 and for NMC-(3:1:1), ΔH_1 ~2000 G, Ni/Mn ~3, correlate well with the EPR analysis reported in the literature [22]. It has been recognized that the considerable EPR line broadening indicates a dipole–dipole or/and exchange interaction between transition metal ions in the layered structure, at least in samples with the high paramagnetic centers concentration. It is worth noting that this phenomenon can occur not only between Mn^{4+}–Mn^{4+} but for Mn^{4+}–Ni^{2+} and Ni^{2+}–Ni^{2+}couples as well.

It can be seen that Al and Fe substitution has markedly influenced the EPR spectrum of the material. In case of NMCAF, the decrease of ΔH_1 due to Al and Fe substitution compared to ΔH_1 for NMC-(3:1:1) cannot be directly linked with the results related to the $\Delta H_1 \sim F(Ni^{2+})$ function introduced in Ref. [25] due to the difference of Ni, Mn and Co stoichiometric ratios. Nevertheless, the results displayed in Fig. 3b and c, show a substantial decrease of R_2 line width related to a corresponding reduction of the Ni^{2+} defect density in NMCAF which is in a good agreement with the results obtained in Ref. [25]. The above discussed observation suggests a redistribution of the Ni ions in the structure induced by the Al and Fe substitution, which can be a reason for the diminished cation mixing in NMCAF.

Unexpectedly, the temperature dependence of the g-factor for NMCAF in the interval 150 K–295 K displayed a rather unusual behavior. In relation to this, it can be assumed that changes in the crystalline field parameters due to the lattice distortion can be the reason for the atypical temperature behavior of the g-factor. Future work will aim to confirm the above hypothesis by performing XRD measurements in the same temperature interval.

Another important feature related to the properties of the single electron states in the material is the paramagnetic–ferromagnetic phase transition, taking place at a characteristic temperature (T_c – Curie point) for a given type of structure. The paramagnetic–ferromagnetic phase transition can be experimentally observed by analyzing the $\Delta H_1 \sim F(T)$ dependence. Typically, the temperature decrease induces a fast enhancement of ΔH, starting at T_c. The results for ΔH_1 temperature evolution for NMC-(3:1:1), NMC-(1:1:1) (Fig. 4c) and NMCAF (Fig. 4a) show that for all types of structures T_c keeps a constant value of about 125 K, being approximately the same as reported for instance in Ref. [25]. Hence, it can be assumed that the stoichiometry change and the Al and Fe substitution do not influence the paramagnetic–ferromagnetic phase transition in the studied materials.

3.3. Material morphology

After synthesis, the morphologies of the non-substituted NMC-(3:1:1) and the substituted material NMCAF have been analyzed by SEM. Fig. 5 shows the SEM images of NMCAF (Fig. 5a, b) and NMC-(3:1:1) (Fig. 5c, d) respectively taken at two different magnifications. The initial material morphology comprises small sub-micrometer sized crystals and big agglomerates consisting of weakly bind smaller crystallites. Detailed SEM analysis of the surface morphology for both NMC-(3:1:1) and NMCAF samples show formation of well-defined rectangular-like shaped crystals with a similar size. The size distributions ranges between 150–500 and 150–600 nm for NMCAF and NMC (3:1:1) correspondingly. Mechanical grinding of the materials was performed before slurry preparation in order to disintegrate the existing agglomerates, after which the morphology displayed exclusively sub-micrometer sized crystal dimensions. Additionally, in order to characterize the actual surface of the materials before their use, B.E.T. specific surface measurements were performed. The results display very similar specific surface for both materials, $S_{B.E.T.} = 4.02\ m^2\ g^{-1}$ for NMC (3:1:1) and $S_{B.E.T.} = 4.21\ m^2\ g^{-1}$ for NMCAF, indicating as well very close size distributions.

3.4. Thermal properties

DTA/TG measurements were used to investigate the thermal stability of the material and to determine the temperature range in which phase transition phenomena occur. Furthermore, DTA/TG tests are used to verify the existence of H_2O or other absorbed/adsorbed components in the structure and to identify the thermal conditions of their release. DTA/TG curves, displaying the thermal behavior of the NMCAF material are presented in Fig. 6.

It can be seen that the DTA measurements show two main peaks. The exothermic peak occurring at 390 °C can be related to the release of carbon dioxide and other residual gases (mainly CO, NO and NO_2), and an endothermic peak occurring at 700 °C, corresponds to the crystallization of the material. The obtained values are very close to the results for other NMC type materials [4]. Additionally, as can be clearly seen on the TG curve, a weight loss of 17%, related to the release of gaseous products in the broad temperature range of the experiment, is observed throughout the thermal treatment. Previous thermal experiments showed that the

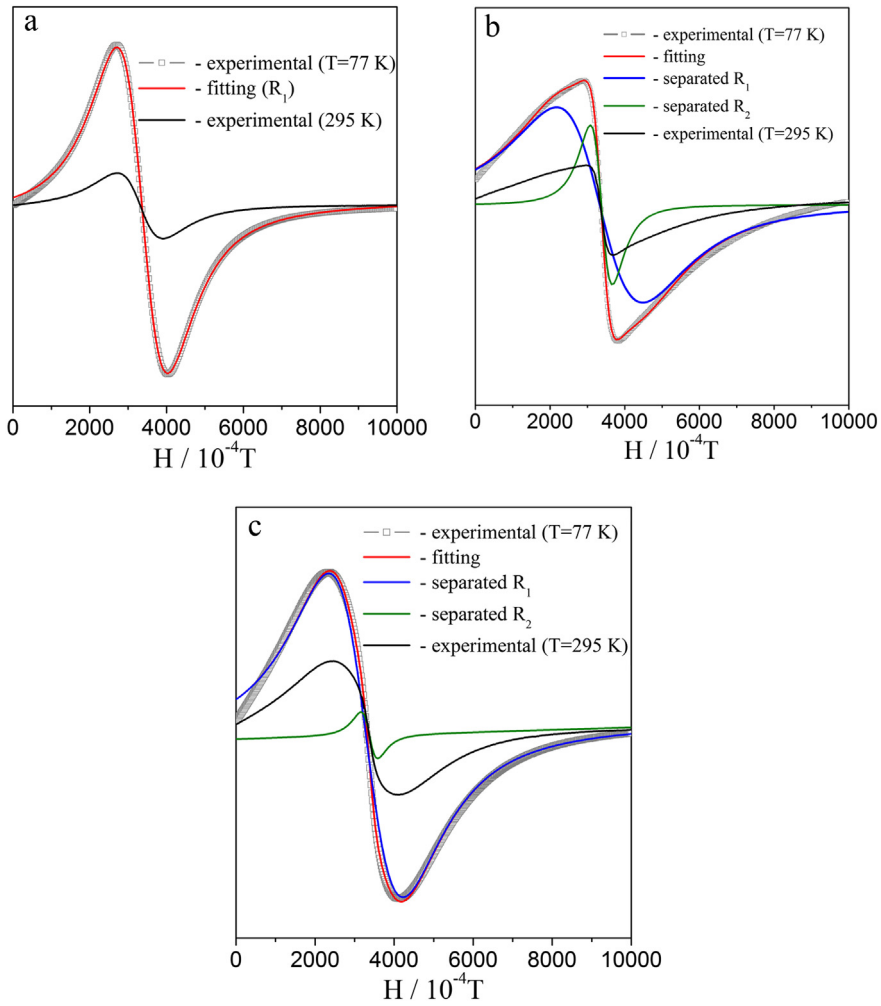

Fig. 3. Experimental EPR spectra of a) NMC-(1:1:1), b) NMC-(3:1:1) and c) NMCAF, recorded at 77 K and 295 K. Fitted and separated after fitting curves are shown for each material.

thermal degradation of these materials is associated with oxygen release [4,26,27].

3.5. Electrochemical performance

The voltammetric behavior of the metal substituted and non-modified material display nearly identical features (Fig. 7). The extraction of Li ions from the lattice occurs at 3.60 V (vs. Li/Li^+) and the main cathodic peak corresponding to the insertion of Li ions is centered at about 3.35 V (vs. Li/Li^+). The voltammetric couple of the electrochemical Li ion exchange presents good reversibility and electrochemical stability upon continuous cycling. The potential difference between anodic and cathodic peak currents is about 0.27 V for NMCAF and 0.25 V for the NMC material, suggesting that both structures have quasi-reversible electrochemical kinetics. Similar voltammetric behavior has been observed for NMC-(1:1:1) [28] and other Li-ion intercalating materials [29]. Furthermore, the positions of oxidation and reduction peaks remain at constant potential with the cycle number, which indicates good stability of the material during voltammetric cycling.

The electrochemical performance of NMCAF and NMC-(3:1:1) was further investigated by galvanostatic cycling at a slow rate C/20 in the potential range between 2.5 and 4.4 V vs. Li/Li^+ (Fig. 8).

It can be seen that both materials display the characteristic for NMC-type structure lithiation–delithiation potential profile. Furthermore, the results indicate that NMCAF delivers an initial discharge capacity of 189 mAh g^{-1}, while for NMC-(3:1:1) the first discharge capacity reaches only 155 mAh g^{-1}, suggesting that the metal substituted structure is able to accommodate a higher amount of Li^+. The galvanostatic cycling reflects the good reversibility of the intercalation/deintercalation process of Li^+ in both layered oxide structures. However, the difference in terms of irreversible capacities between the substituted and non-substituted materials, 71 mAh g^{-1} and 81 mAh g^{-1} respectively, indicates that NMCAF is more stable during the first charge than NMC-(3:1:1). The observed irreversible capacity for these types of materials is usually attributed to instabilities of the electrode surface towards electrolyte components at high potentials [30]. Besides, the NMCAF sample also shows superior capacity retention (89.9%) after 10 cycles compared to NMC-(3:1:1) (86.5%).

Next to the capacity increase, visible changes in plateau potentials are observed after the metal substitution. The plateau potential can be changed as a consequence of a chemical potential shift caused by Fe and Al substitution, in case of major deviation of the active for intercalation amount, increase of the layer resistance or other related reasons causing potential polarization. In order to compare properly the lithiation and de-lithiation potentials, taking into consideration as well the state-of-charge of the active for intercalation material we have presented the galvanostatic curves after capacity normalization (Fig. 8c). At these conditions the potential differences can be displayed at corresponding constant degree of lithiation. It can be seen that the plateau potentials for Li^+

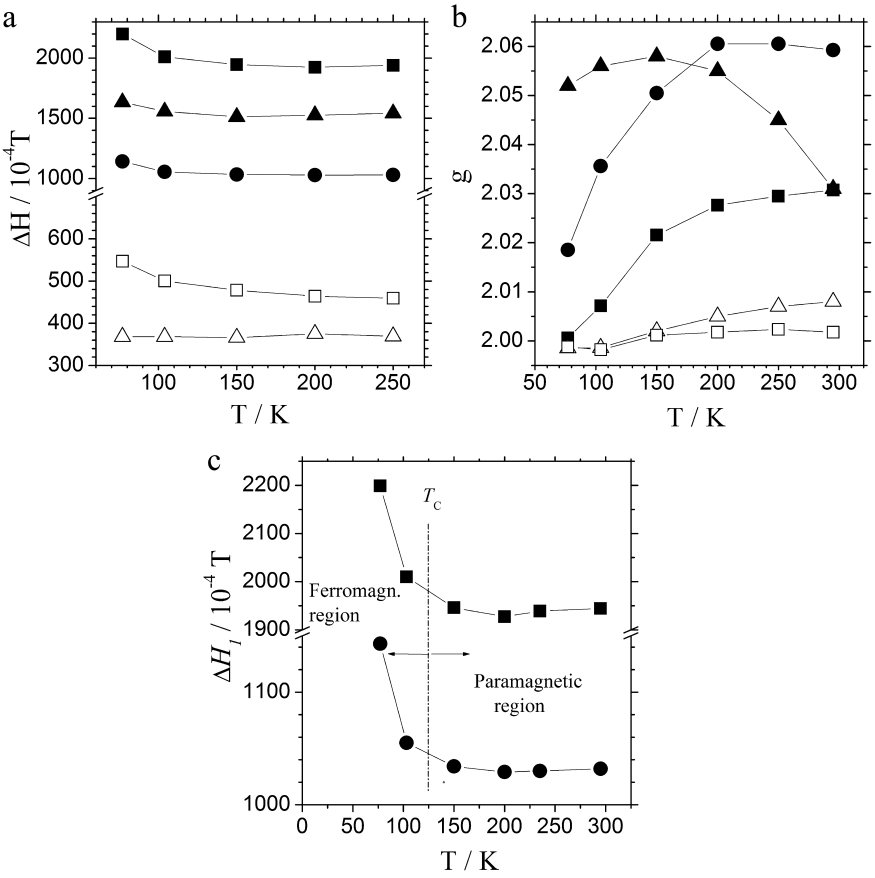

Fig. 4. ΔH (a) and g (b) as a function of temperature. Closed symbols denote ΔH_1 and g_1, (■)-NMC-(3:1:1), (▲)-NMCAF, (●)-NMC-(1:1:1) and open symbols denote ΔH_2 and g_2 (□)-NMC-(3:1:1); (Δ)-NMCAF. (c) – representation of paramagnetic–ferromagnetic phase transition for (■)-NMC-(3:1:1) and (●)-NMC-(1:1:1).

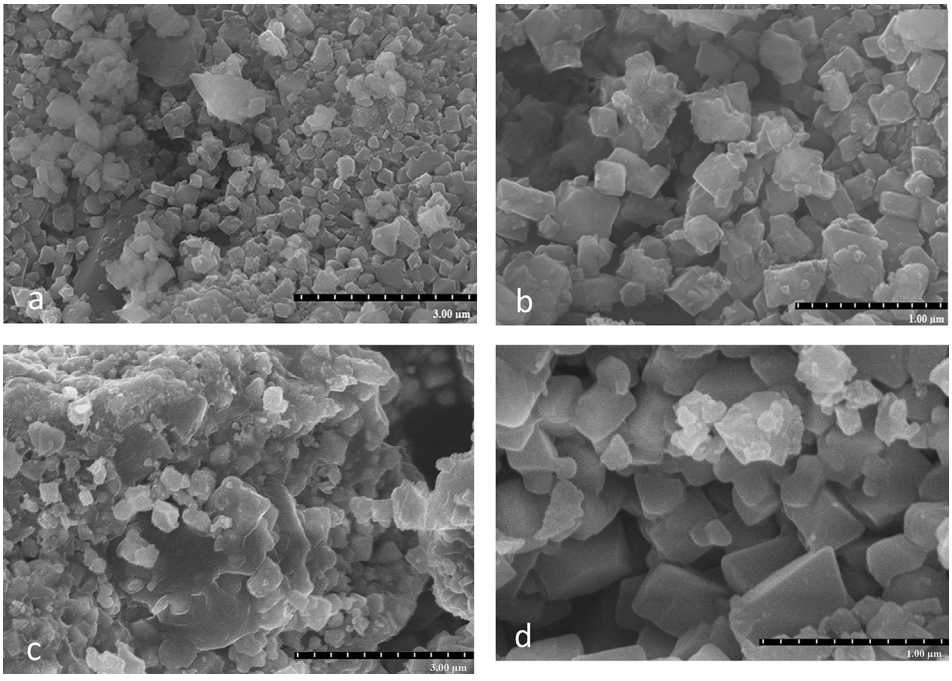

Fig. 5. SEM images of NMCAF (a, b) and NMC-(3:1:1) (c, d), at low (a, c) high (b, d) magnifications.

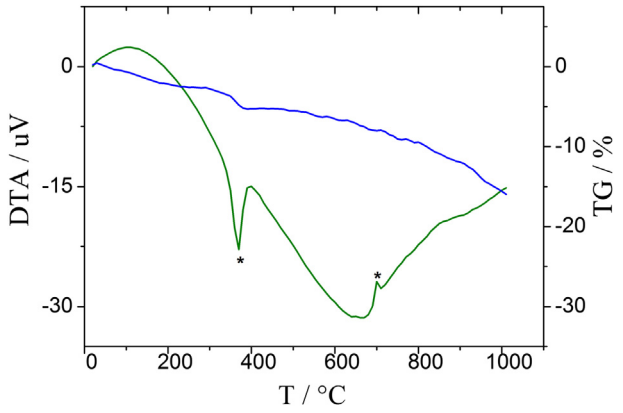

Fig. 6. DTA (green)–TG (blue) curves of NMCAF, measured after self-combustion, before annealing at high temperature. (For interpretation of the references to colour in this figure legend, the reader is referred to the web version of this article.)

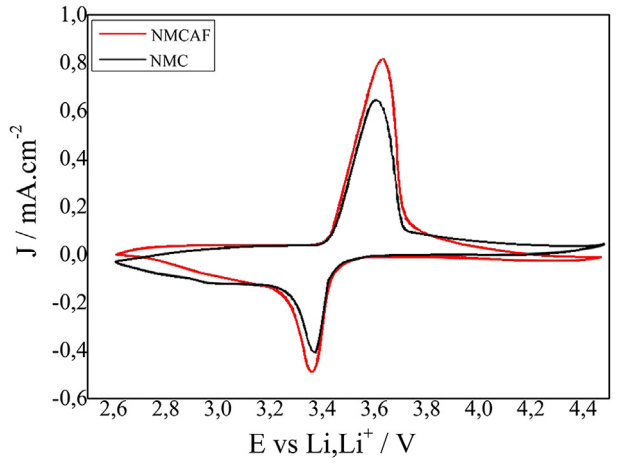

Fig. 7. Cyclic voltammograms of NMC-(3:1:1) (black) and NMCAF (red) positive electrode materials. $v = 100\ \mu V\ s^{-1}$. (For interpretation of the references to color in this figure legend, the reader is referred to the web version of this article.)

insertion increased and for de-insertion decreased in almost entire charge–discharge interval. Practically, this result suggests that after the substitution both processes are stimulated since less energy is required for exchange of a certain amount of Li^+. The major difference in the potentials (about 200 mV) was detected at 25% Li insertion. It is here important to emphasize that this big change has been induced by a very small doping (2.5% of each element). The effect of considerable voltage change stays in a good correlation with the change of the structural parameters after the substitution, extracted by Rietveld refinement (Table 1). Whereas the lattice parameters have changed minimally (0.2–0.6%) in accordance with the low degree of substitution, the occupancy of Ni^{2+} in Li^+ sites remarkably decreased with more than 60%. The last observation suggests that metal substitution increases the order in the structure, providing possibility for easier and more efficient Li^+ intercalation, since the degree of cation mixing is decreased. This effect can be the reason for the potential shifts of insertion/de-insertion plateaus. Furthermore, from electrochemical and thermodynamic point of view at equilibrium, the potential of the cell at open circuit ($E^{+}_{OCP\ vs.\ Li,Li}$) depends on the difference between the standard potentials of both electrodes, which is a function of the chemical potentials (free energies) of the active components. Therefore, the difference in E_{OCP} can be a quantity for estimation of electrochemical potential change after the metal substitution, without interference of any polarization effect. Our results have shown that the initial E_{OCP} of NMCAF has lower value ($E_{OCP,\ NMCAF} = 2.0$ V) than E_{OCP} of NMC-(3:1:1) ($E_{OCP,\ NMC\ (3:1:1)} = 2.8$ V), suggesting much easier oxidation of NMCAF than NMC-(3:1:1). The E_{OCP} displayed stable values and difference in E_{OCP} between two materials has been observed as well before starting further galvanostatic or voltammetric measurements. On the other hand, we have proven that the material structure has been definitely reorganized after the substitution and significant decrease of the cation mixing has been achieved. Therefore, it is highly expected that the transformation in the local Ni^{2+} environment, facilitating the kinetics of Li^+ exchange has the dominating impact for the electrochemical performance improvement.

Previous work on Al- and Fe-substituted NMC (1:1:1) has been conducted in order to assess the impact of Fe and Al doping on the electrochemical performance of material [5]. The plateau potential variations for $LiNi_{1/3}Co_{1/3-x}Fe_xMn_{1/3}O_2$ and $LiNi_{1/3}Co_{1/3-x}Al_xMn_{1/3}O_2$ have been interpreted in terms of drop of chemical potential of the material in case of Al and polarization effect for Fe substitution. The effect of the metal doping on plateau potential was however observed at relatively high Al and Fe amounts $x > 0.11$. In contrast, our results show that for the Ni-rich stoichiometry NMC (3:1:1), a very small addition of dopant (Al and Fe) $x = 0.025$ induces considerable structural stabilization and strong performance improvement. Furthermore, opposite to our case, the effect of Fe and Al substitution in NMC (1:1:1) on material capacity and delithiation potential was shown to be reverse [5]. Most likely in this case, other types of mechanisms govern the structural transformation. The physical origin for the difference between these two effects will be investigated in our next upcoming work.

The long term galvanostatic cycling performance of NMCAF at faster rates (C/5 and C) is shown in Fig. 9.

It can be observed that the discharge capacity during long term galvanostatic cycling is rather high. Especially for the first 20 cycles, the capacity retention is 90% for both C/5 and 1C rates. Nevertheless, after 100 cycles a significant difference in capacity retention between the two C rates can be observed. The retention values of 75.4% for C/5 and 61.4% for 1C achieved after 100 cycles demonstrate superior cycling behavior of the metal ion substituted material. The excellent capacity and cycling performance for Al and Fe substituted NMC structure can be related to the existence of the Fe–O bond in the host structure which is available for the intercalation of Li^+ ions [31]. In addition, it was observed that the extra amount of nickel ions in the interlayer space that should normally be occupied by lithium ions, is lower for NMCAF compared to NMC-(3:1:1). These extra Ni^{2+} ions cause repulsions with the Li^+ ions during the discharge process (Li^+ insertion), resulting in a decline in the specific capacity and regress in the material performance. Furthermore, the above observation is in good accordance with the EPR data, which showed indications for rearrangement of the local environment of the transition metals in the NMCAF structure.

4. Conclusion

The method of self-combustion synthesis was applied to prepare double Al- and Fe-substituted cathode material with the stoichiometry $LiNi_{0.6}Mn_{0.2}Co_{0.15}Al_{0.025}Fe_{0.025}O_2$ (NMCAF). The novel NMCAF material displayed an improved capacity and high stability during electrochemical cycling.

Structural characterization by means of XRD showed that NMCAF crystallizes in the α-$NaFeO_2$ type structure. The lattice parameters a and c are larger for NMCAF (2.868 Å and 14.211 Å respectively) than for the non-substituted material NMC-(3:1:1), 2.861 Å and 14.167 Å respectively) due to the cationic substitution of Co^{3+} by Fe^{3+}.

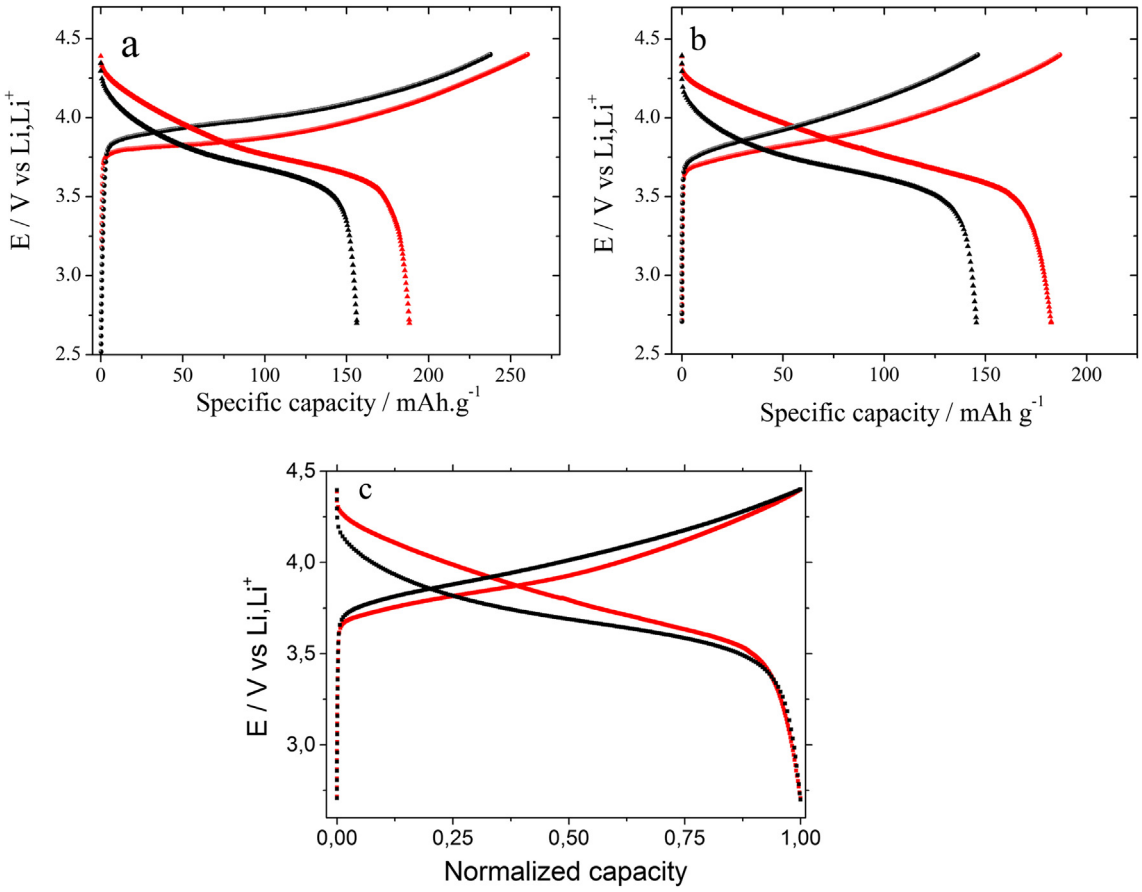

Fig. 8. Galvanostatic cycling at C/20 rate of NMC-(3:1:1) (black) and NMCAF (red) positive electrode materials a) 1st cycle, b) 10th cycle, c) comparison of voltage profiles vs. normalized capacity for the 10th cycle. (For interpretation of the references to color in this figure legend, the reader is referred to the web version of this article.)

Electron paramagnetic resonance (EPR) spectroscopy showed that Al and Fe substitution significantly influenced the EPR spectrum of NMC-(3:1:1). The EPR signals of both materials are attributed to Mn^{4+} and Ni^{2+} present in the structure. The change in the Ni^{2+} line after the metal substitution suggests a redistribution of the Ni ions in the layered structure, which can be the reason for the diminished cation mixing in the NMCAF.

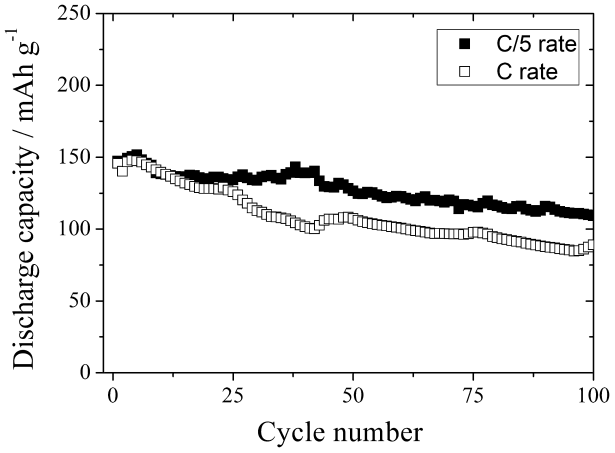

Fig. 9. Specific discharge capacities of the NMCAF material dependent on cycle number at two different C rates.

The cyclic voltammetry and the galvanostatic cycling measurements indicate that NMCAF allows a better lithium intercalation and de-intercalation process. It presents a discharge capacity in the order of 189 mAh g^{-1} (C/20), and a high capacity retention even at moderately fast rates (C/5 and C), which is comparable to some of the best ever reported electrochemical properties of NMC type materials. The improved electrochemical behavior of NMCAF is closely connected to the stabilization of the structure and the reduction of the cation mixing after cationic substitution.

Acknowledgment

Financial support by the DFG funded program WeNDeLIB (project 6: "Linking of model and commercial active materials for lithium ion batteries by in situ determination of thermodynamic and kinetic data"), by a grant (NanoBatt TNA VII-1/2012) from the state of Thuringia (TMWAT by LEG Thuringen), co-financed by the European Union with in the frame of the European Funds for Regional Development (EFRD) and as well the financial support from the State of Thuringia (grant for W. El Mofid) is gratefully acknowledged.

Thanks are due to Dr. S. Upadhyayula, chemical engineering department, I.I.T. Delhi for the help with the B.E.T. measurements.

References

[1] Y. Chen, G.X. Wang, K. Konstantinov, H.K. Liu, S.X. Dou, J. Power Sources 119–121 (2003) 184.
[2] B.J. Hwang, Y.W. Tsai, D. Carlier, G. Ceder, Chem. Mater. 15 (2003) 3676–3682.

[3] T. Ohzuku, Y. Makimura, Chem. Lett. 7 (2001) 642–646.
[4] H.-J. Noh, S. Youn, C. Yoon, Y.-K. Sun, J. Power Sources 233 (2013) 121–130.
[5] D. Liu, Z. Wang, L. Chen, Electrochim. Acta 51 (2006) 4199–4203.
[6] X. Zhang, W. Jiang, A. Mauger, F. Gendron, C. Julien, J. Power Sources 195 (2010) 1292–1301.
[7] T. Ohzuku, A. Ueda, M. Kouguchi, J. Electrochem. Soc. 142 (1995) 4033.
[8] A. Ueda, N. Nagayama, Y. Iwakoski, H. Komori, Electrochim. Acta 38 (1993) 1159.
[9] Y. Meng, Y. Wu, B.-J. Hwang, Y. Li, G. Ceder, J. Electrochem. Soc. 151 (2004) A1134.
[10] B. Zhang, L. Li, J. Zheng, J. Alloys Compd. 520 (2012) 190.
[11] Y. Idemoto, N. Kitamura, K. Ueki, S.C. Vogel, Y. Uchimoto, J. Electrochem. Soc. 159 (2012) A673.
[12] W. Luo, F. Zhou, X. Zhao, Z. Lu, X. Li, J. Dahn, Chem. Mater. 22 (2009) 1164.
[13] T. Fey, C. Chang, T. Kumar, J. Solid State Electrochem. 14 (2010) 17.
[14] J. Dou, X. Kang, T. Wumaier, H. Yu, N. Hua, Y. Han, G. Xu, J. Solid State Electrochem. 16 (2012) 1481.
[15] K. Yang, L.Z. Fan, J. Guo, X. Qu, Electrochim. Acta 63 (2012) 363.
[16] Z. Yang, Z. Song, G. Chu, X. Kang, T. Ren, W. Yang, Q. Qiao, J. Mater. Sci. 47 (2012) 4205.
[17] I. Saadoune, M. Dahbi, M. Wikberg, T. Gustafsson, P. Svedlindh, K. Edström, Solid State Ionics 178 (2008) 1668–1675.
[18] J. Rodriguez-Carvajal, Fullprof, Program for Rietveld Refinement, Version 3.7, LLB JRC, 1997.
[19] Y. He, L. Pei, X. Liao, Z. Ma, J. Fluor. Chem. 128 (2007) 139–143.
[20] R. Gummow, M. Thackeray, W. David, S. Hull, Mater. Res. Bull. 27 (1992) 327.
[21] T. Ohzuku, A. Ueda, M. Nagayama, J. Electrochem. Soc. 140 (1993) 1862.
[22] H. Sclar, D. Kovacheva, E. Zhecheva, R. Stoyanova, R. Lavi, G. Kimmel, J. Grinblat, O. Girshevitz, F. Amalraj, O. Haik, E. Zinugrad, B. Markovsky, D. Aurbach, J. Electrochem. Soc. 156 (2009) A939–A948.
[23] R. Stoyanova, A.-L. Barra, M. Yoncheva, E. Zhecheva, E. Shinova, P. Tzvetkova, S. Simova, Inorg. Chem. 49 (2010) 1032–1941.
[24] E. Zhecheva, R. Stoyanova, R. Alcantara, P. Lavela, J. Tirado, J. Power Sources 174 (2007) 519–523.
[25] A. Mauger, F. Gendron, C. Julien, J. Alloys Compd. 520 (2012) 42–51.
[26] J. Dahn, E. Fuller, M. Obrovac, U. von Sacken, Solid State Ionics 69 (1994) 265–270.
[27] M. Guilmard, L. Croguennec, D. Denux, C. Delmas, Chem. Mater. 15 (2003) 4476–4483.
[28] C. Rao, A. Reddy, Y. Ishikawa, P. Ajayan, Appl. Mater. Interfaces 3 (2011) 2966–2972.
[29] M. Takahashi, S. Tobishima, K. Takei, Y. Sakurai, Solid State Ionics 148 (2002) 283–289.
[30] J. Choi, A. Manthiram, Electrochem. Solid-State Lett. 8 (2005) C102–C105.
[31] H. Li, G. Chen, B. Zhang, J. Xu, Solid State Commun. 146 (2008) 115–120.